WATER RESOURCES RESEARCH, VOL. 49, 5411–5426, doi:10.1002/wrcr.20372, 2013

Quantifying groundwater-surface water interactions in a proglacial moraine using heat and solute tracers

Gregory Langston,[1,2] Masaki Hayashi,[1] and James W. Roy[1,3]

Received 31 October 2012; revised 24 April 2013; accepted 18 June 2013; published 5 September 2013.

[1] Recent studies in mountain environments have indicated that groundwater represents a major component of the water balance of alpine streams and lakes. However, the scarcity of information on the hydraulic properties of geological materials in alpine environments presents a major obstacle to understanding the response of these watersheds to hydrological inputs and their future variability. The information is particularly limited for talus and proglacial moraine, where rugged topography prohibits the installation of groundwater monitoring wells. Observation of groundwater-surface water interaction provides a useful tool for studying groundwater in these challenging environments. Here we present a unique experiment using a tarn (i.e., pond on proglacial moraine) in a partially glaciated watershed in the Canadian Rockies as a surrogate for a groundwater monitoring well. A chloride dilution test and detailed energy balance monitoring were simultaneously conducted to quantify the groundwater-surface water interactions. The water balance of the tarn was dominated by groundwater inflow and outflow, ranging between 70 and 720 m^3 d^{-1}, while the volume of the water in the tarn fluctuated between 140 and 620 m^3. Comparing the observed flow rates with a semianalytical solution of groundwater interactions with a flow-through pond, the hydraulic conductivity of the proglacial moraine is estimated to be in the order of 10^{-3} m s^{-1}, which provides one of the very few measurements of large-scale hydraulic conductivity of proglacial moraine. The study demonstrates a useful application of mass and energy balance measurements in rugged environments and provides the essential information for advancing our understanding of alpine groundwater hydrology.

Citation: Langston, G., M. Hayashi, and J. W. Roy (2013), Quantifying groundwater-surface water interactions in a proglacial moraine using heat and solute tracers, *Water Resour. Res.*, *49*, 5411–5426, doi:10.1002/wrcr.20372

1. Introduction

[2] Alpine watersheds represent an important source of freshwater for many regions of the world [*Viviroli et al*., 2007]. As both climate and water demands change, an improved understanding of the hydrological processes in alpine environments will be critical for developing effective water management strategies [*Barnett et al*., 2005].

[3] Recent studies have shown that groundwater plays an important role in the hydrologic cycle of alpine watersheds. Using chemical and isotopic analysis *Liu et al*. [2004] showed that groundwater flow contributes more than two thirds of streamflow at two study locations in the Colorado Rockies. Similarly, using isotopic analysis *Baraer et al*. [2009] showed that groundwater is the largest contributor to basin outflow during the dry season in Cordillera Blanca in Peru. Detailed water-balance studies showed that groundwater is also a significant component of the water balance of several alpine lakes in the Lake O'Hara research area in the Canadian Rockies [*Hood et al*., 2006; *Roy and Hayashi*, 2008]. At a much larger scale, *Andermann et al*. [2012] observed a delay in the response of discharge to precipitation and snowmelt input in Himalayan rivers, and attributed the cause of delay to groundwater storage and release. Furthermore, groundwater also plays an important role in groundwater-dependent ecosystems at high elevations, such as mountain meadows [*Lowry et al*., 2011].

[4] Coarse deposits, such as moraines, rock glaciers, and talus, are thought to play a significant role in the transport and storage of groundwater in alpine headwater regions. Talus slopes were identified as the primary groundwater reservoirs at a study site in the Colorado Rockies, where groundwater discharging from these deposits accounted for >75% of storm streamflow and winter base flow [*Clow et al*., 2003]. In the Lake O'Hara research area, *Roy and Hayashi* [2008, 2009] showed that a proglacial moraine deposit is an important source of groundwater for both an alpine lake and for the major outlet stream of the watershed, while talus slopes were suggested as important for groundwater flow to two other lakes [*Hood et al*., 2006; *Roy and*

[1]Department of Geoscience, University of Calgary, Calgary, Alberta, Canada.
[2]Alberta Environment and Sustainable Resources Development, Edmonton, Alberta, Canada.
[3]National Water Research Institute, Environment Canada, Burlington, Ontario, Canada.

Corresponding author: M. Hayashi, Department of Geoscience, University of Calgary, 2500 University Dr. NW, Calgary, AB T2N 1N4, Canada. (hayashi@ucalgary.ca)

0043-1397/13/10.1002/wrcr.20372

Hayashi, 2008]. Infiltration of glacier meltwater into sloped talus and moraine features was observed in the Cordillera Real, Bolivia, with springs forming at their base only during the wet season [*Caballero et al*., 2002]. A recent study in the Swiss Alps indicated the strong interaction between groundwater and the glacier-fed streams flowing over the proglacial moraine [*Magnusson et al*., 2013].

[5] In addition, results from several studies using water chemistry suggest multiple distinct flow paths occur in these coarse deposits, with these flow systems classified by their response times (e.g., fast versus slow response flow systems) [*Krainer and Mostler*, 2002; *Brown et al*., 2006; *Williams et al*., 2006; *Roy and Hayashi*, 2009]. These studies suggest that a slow response system is likely the result of deeper groundwater flow, whereas a fast flow likely represents shallow subsurface flow along impermeable boundaries such as buried ice and near-surface bedrock [*Tenthorey*, 1992; *Brown et al*., 2006; *Williams et al*., 2006]. The groundwater response time in the alpine headwater regions are usually not considered in the "transit time" of glacier meltwater before they enter the river systems [e.g., *Huss*, 2011]. However, the hydraulic response time of deeper groundwater flow systems may be significant enough to affect the overall response of mountain rivers to glacier and snowmelt, and should be considered in hydrological models.

[6] To incorporate groundwater transit times into these models in a quantitative way requires information on groundwater flow rates and the hydraulic properties (e.g., hydraulic conductivity, storativity) of coarse deposits. However, this is a key knowledge gap in the current understanding of alpine groundwater systems. Indeed, *Tague and Grant* [2009] state that the scarcity of accurate data on hydraulic properties is a major obstacle to understanding the response of alpine streamflow to climate change. This lack of information is largely the result of the challenging alpine environment, which makes it logistically difficult and prohibitively costly to install monitoring wells and other infrastructure. Consequently, other methods for investigating the groundwater flow systems within coarse deposits are required.

[7] One method that has been employed in a few cases is monitoring the transit time of field-applied tracers across or through the coarse deposits. In one of very few studies to examine water flow rates through rock glaciers, *Krainer and Mostler* [2002] employed dye-tracer experiments to study three rock glaciers in Austria. Their results suggest that groundwater moved through two distinct storage reservoirs, and they hypothesized that both a quick flow and base flow systems were present. They interpreted flow velocities of 0.015–0.037 m s^{-1} to represent channeled flow in the quick flow response system (shallow groundwater flow in contact with ice). Base flow was reported to be relatively minor in these systems and these flow rates were not quantified. Another study of groundwater flow through rock glaciers also employed a tracer test on three rock glaciers in the Alps [*Tenthorey*, 1992]. This study suggested fast "supraflow" velocities of 0.058 m s^{-1} and "intraflow" velocities of 0.0002–0.0004 m s^{-1}. Deeper groundwater flow traveled slower than intraflow, but again velocities were not quantified. To our knowledge, very few tracer tests have been conducted on proglacial moraines, with an exception of *Caballero et al*. [2002], who conducted a salt tracer test on the lateral moraine of a Glacier in Bolivia and determined a groundwater flow velocity of 0.0003 m s^{-1}. Determination of hydraulic properties was not made in these three studies.

[8] Another potentially useful method that has not been reported to date is assessing groundwater flow rates and hydraulic properties by studying groundwater-surface water (GW-SW) interactions. Because surface water is an expression or "outcrop" of the groundwater system, studying GW-SW interactions can provide useful information regarding the groundwater system [*Siegel*, 2008]. These interactions can be quantified through water balances, although the water balance alone cannot readily distinguish the groundwater components. To do so requires the monitoring of a tracer, which could include a natural tracer such as heat or an introduced chemical tracer.

[9] Heat is an effective natural tracer that has been used to determine groundwater seepage flux across streambeds, and to delineate gaining and loosing reaches of streams [*Conant*, 2004; *Anderson*, 2005; *Hatch et al*., 2006; *Schmidt et al*., 2007; *Constantz*, 2008]. The advection of thermal energy by groundwater to lakes is commonly assumed to be a negligible component of lake energy balance [*Rodríguez-Rodríguez et al*., 2004; *Elo*, 2007; *Rouse et al*., 2008], but has been shown to play a significant role in the energy balance of a proglacial lake [*Chikita et al*., 2000]. It seems plausible that for small alpine lakes and tarns that are heavily influenced by groundwater, the advection of heat by groundwater could play an important role in the lake energy balance. If so, a detailed energy-balance study could provide useful information regarding groundwater flow rates through coarse deposits connected to these small water bodies.

[10] Artificial chemical tracers have also been used effectively to investigate GW-SW interactions [*Kalbus et al*., 2006]. *Parsons et al*. [2004] performed a whole-wetland tracer experiment to investigate infiltrations in a prairie wetland. A chemical mass-balance approach has been used to measure groundwater exchange with alpine lakes in Montana [*Gurrieri and Furniss*, 2004] and to estimate groundwater seepage to and from a closed-basin lake [*LaBaugh et al*., 1997]. However, *LaBaugh et al*. [1997] noted that seepage-rate estimates based on the chemical mass balance did not agree with values determined from flow nets and isotope analysis. They therefore suggested using a combination of chemical mass balance with other approaches to estimate seepage rates.

[11] This paper reports a unique experiment that uses a tarn (i.e., small pond connected to the proglacial moraine aquifer) as a surrogate for a groundwater monitoring "well" to conduct a chloride tracer dilution test and a detailed energy balance (heat as the tracer) to quantify GW-SW interactions. The primary objectives are to demonstrate the use of this approach for: (1) determining the complete water balance for the tarn, including groundwater flow into and out of the tarn and (2) estimating the hydraulic conductivity of the proglacial moraine at a scale of the tarn (~50 m). These are critical information for assessing the importance of groundwater processes in coarse sediments typical of alpine headwater basins and for incorporating the proglacial moraine as a hydrological response unit in future hydrological modeling efforts.

2. Study Site

[12] The study area is located in the Lake O'Hara watershed in Yoho National Park, British Columbia, Canada (Figure 1a). The elevation of the watershed ranges from 2050 to 3490 m.a.s.l. and is characterized by rugged subalpine and alpine terrain. By area, the watershed is ~60% moraine and talus deposits, 25% exposed bedrock, and 15% alpine meadow and subalpine forest. Bedrock in this region is composed primarily of thickly bedded quartzite and quartzose sandstone, separated by thin layers of siltstone, sandstone, and gray shale of the Cambrian Gog Group. Carbonate rocks of Mt. Whyte, Cathedral, Stephen and Eldon Formations are present in the moraine and talus material [*Price*, 1980; *Lickorish and Simony*, 1995]. A small glacier (the Opabin glacier) is located at the southern end of the study area (Figure 1b) and is separated from the rest of the study area by a large moraine complex. The moraine surface material is dominated by large boulders with gravels and coarse sands (0.5–1 mm in diameter) [*Langston et al*., 2011], and there does not appear to be systematic spatial variability in sediment grain size. Due to the coarse grain size and high hydraulic conductivity of the moraine material, all snowmelt, glacier melt, and rain that occurs on or upslope of the moraine infiltrates within a very short distance and is then transported through the moraine as groundwater. Groundwater from the moraine is discharged from a series of springs located at its western terminus (Figure 1b). Groundwater may also discharge into Opabin Lake before being rerouted back through the lower moraine to the groundwater springs [*Roy and Hayashi*, 2009]. Geophysical and visual evidence show that regions of the moraine have ground ice [*Langston et al*., 2011]. Groundwater flow paths through the moraine are hypothesized to be controlled primarily by bedrock topography and ground ice, where it exists [*Langston et al*., 2011].

[13] This study focuses on a small tarn located on the eastern edge of the moraine (hereafter East Tarn; Figures 1b and 1c). The depth to the bedrock under the tarn is estimated to be 10 m based on previous geophysical survey data using electrical resistivity tomography (ERT) and ground penetrating radar (GPR) [*Langston et al*., 2011; *McClymont et al*., 2012]. There are no surface water inflows or outflows to the tarn (Figure 1d), and yet *Roy and Hayashi* [2008] reported strong daily water level fluctuations in response to melting of Opabin glacier or snow far from the tarn, suggesting groundwater inflow and outflow.

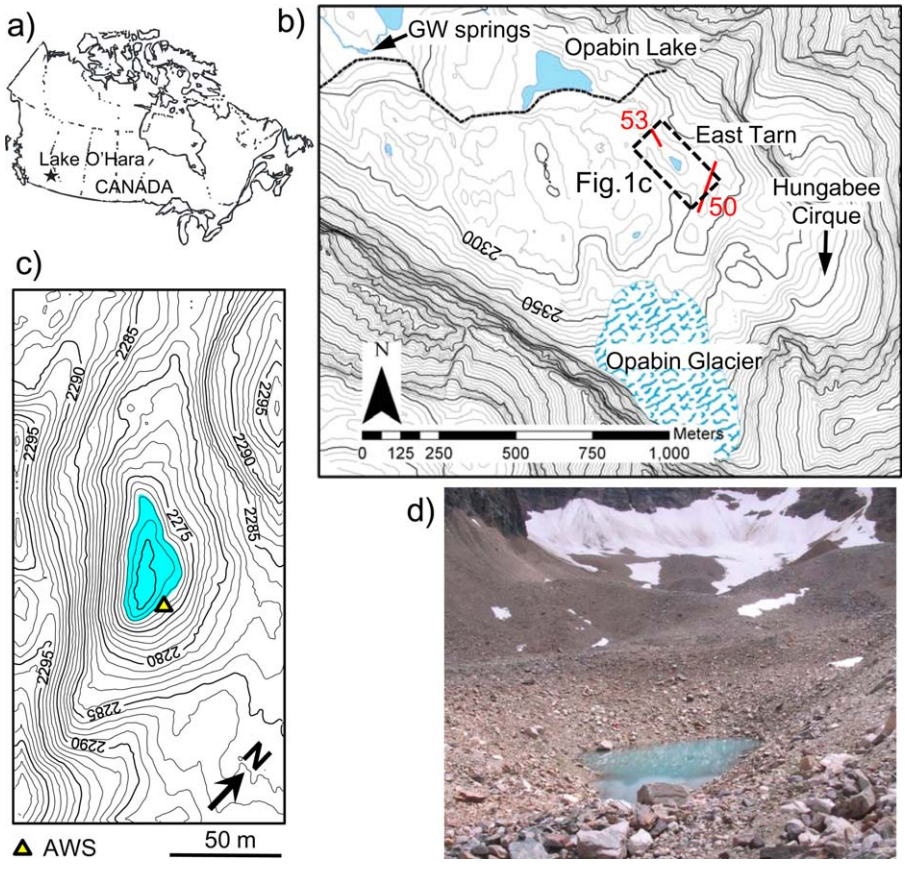

Figure 1. (a) The location of the study area in Canada. (b) The Opabin glacier and moraine complex including the East Tarn and a number of other surface water features. The terminus of the moraine is delineated by the thick dashed line. Red lines with numbers indicate GPR survey lines of *McClymont et al*. [2012]. (c) A close-up view of the East tarn with 1 m elevation contours and the location of automatic weather station (AWS). The blue-shaded region indicates the maximum extent of the pond during the 2008 field season. (d) Photograph of the East Tarn looking southeast direction on 29 July 2008, showing the late-lying snowpack in the Hungabee Cirque.

More recent work [*Langston et al*., 2011] indicated that the tarn water level is representative of the local water table. *McClymont et al*. [2012] observed the water table at an elevation close to that of the tarn water level in two GPR survey lines in the vicinity of the tarn (see Figure 1b for location). These findings suggest the East Tarn is a flow-through tarn (i.e., simultaneously receiving and gaining groundwater). The tarn is ephemeral, generally holding water from the beginning of July to mid-September. Thus, the local water table seems to drop below the bottom of the tarn toward the end of the summer season. The tarn is snow-covered prior to the beginning of July, but likely contains some water below the snow, as the local water table rises in response to spring and early summer snowmelt.

3. Methods

3.1. Water Balance

[14] A water balance approach was used to investigate the GW-SW interactions occurring at the East Tarn. Since there are no surface water inflows or outflows to the tarn, the water balance equation simplifies to:

$$\Delta V = P–E + GW_{in}–GW_{out} \quad (1)$$

where ΔV (m^3) is the change in tarn water volume, P (m^3) is the precipitation received at the tarn surface, E (m^3) is evaporation from the tarn surface, GW_{in} (m^3) is the groundwater inflow, and GW_{out} (m^3) is the groundwater outflow. Overland flow is not included as an input to the tarn in equation (1) because it was never observed during the study period even when upslope areas were generating snowmelt.

[15] The volume and area of water in the tarn were derived from water depth measurements and a detailed digital elevation model (DEM) of the area (Figure 1c). Tarn water depth was measured every 10 min with a vented pressure transducer (In-situ Inc., Level Troll). The detailed elevation survey of the East Tarn basin was conducted using a differential global positioning system (DGPS) on 10 September 2008, when the water level was sufficiently low to enable surveying the tarn bottom. The DGPS data of the tarn basin were merged with the high-resolution elevation data of the surrounding area derived from the light detection and ranging (LiDAR) survey data [*Hopkinson et al*., 2009] to generate the detailed DEM. The water depth (h)–area (A)–volume (V) relationship of the tarn was derived from the DEM following the method outlined by *Hayashi and van der Kamp* [2000] as:

$$A = s(h/h_0)^{2/p} \quad (2)$$

$$V = s(h/h_0)^{1+2/p}/(1 + 2/p) \quad (3)$$

where s (m^2) is a scaling parameter, p is a dimensionless parameter related to the average shape of basin profile, and h_0 is the unit depth (= 1 m). The least-squares best fit values of s and p were 256 m^2 and 1.68, respectively, which gave relative root-mean-squared errors (RMSE) of 3.5% for depth-area relation and 1.5% for depth-volume relation.

[16] Precipitation was measured using a tipping bucket rain gauge located ~1 km northwest of the tarn. The volume contribution of precipitation to the tarn was calculated as the amount of precipitation multiplied by the area of the tarn surface. Evaporation from the tarn surface was measured using a floating evaporation pan with a surface area of 700 cm^2. Volumetric evaporation was then calculated using the average daily surface area of the tarn and the daily measured evaporation rate.

[17] The water balance equation (equation (1)) alone cannot distinguish the two unknown groundwater components (GW_{in} and GW_{out}). To do so, it was solved simultaneously with a chloride mass balance equation or an energy balance equation (see below).

3.2. Chloride Mass Balance

[18] A chloride dilution experiment was conducted during 3–8 August 2008 to determine the groundwater components of the tarn water balance. Chloride concentration in the tarn was increased by a one-time injection of 44 kg of sodium chloride (NaCl) on 3 August, using a method similar to that described by *Parsons et al*. [2004]. The NaCl was dissolved in 20 L pails of tarn water before being transferred in solution to seven, 20–30 L containers with spigots. The solution was then distributed over the tarn surface as evenly as possible by draining the solution through the spigots while paddling around the tarn. This took ~1 h to perform. After all the solution was added, the tarn was mixed by vigorous paddling before being left to equilibrate.

[19] The chloride mass balance within the tarn can be calculated as follows:

$$\Delta(C_{tarn}V) = C_P P–C_{GWout}GW_{out} + C_{GWin}GW_{in} \quad (4)$$

where C is the chloride concentration with subscripts indicating precipitation, the tarn water, and groundwater inflow and outflow. Thus, $\Delta(C_{tarn}V)$ is the change in chloride mass in the tarn, C_pP is the chloride mass contribution from precipitation, $C_{GWout}GW_{out}$ is the chloride mass loss from groundwater outflow, and $C_{GWin}GW_{in}$ is the chloride mass contribution from groundwater inflow. Other processes of mass exchange such as dispersion or density-driven flow are considered negligible. This is a reasonable assumption because the lateral groundwater inflow and outflow and associated advection dominate the water and mass balance of the tarn (see section 4 and Appendix A). Groundwater chloride concentration (C_{GWin}) was assumed to be constant and equal to the concentration of the tarn on 2 August (1.3 mg/L), determined as described below. Estimation of C_{GWout} will be described in section 4.

[20] Tarn chloride concentration was determined throughout the tarn volume from the direct measurement of water samples at 18 selected locations within the tarn, and indirectly from the measurement of electrical conductivity (EC) for all other locations. Samples were collected daily, using a prerinsed syringe and flexible plastic tubing, from three depths (the center of the bottom third, middle third and top third of the water column) at six marked locations. Water sampling started the day before the NaCl was added (2 August) and continued until the chloride concentration returned to background levels (9 August). Each sample was

filtered in the field using a 0.45 μm disposable filter, and sample bottles were rinsed three times with filtered sample water before use. Water temperature and EC were measured for each sample. EC measurements were corrected to 25°C [*Hayashi*, 2004]. Chloride concentration was determined using ion-exchange chromatography. Linear relationships between EC and chloride concentration were determined for each day of the experiment using the chloride concentration of water samples and the corresponding EC measurements. These relationships were used to convert EC measurements to chloride concentrations at the 38–44 monitoring locations where samples were not collected (see below). The relative RMSE for each relationship ranged from 12 to 15%, with the exception of 7 August, for which it was 21%.

[21] To account for spatial variability in chloride concentration within the tarn, transects of EC and temperature measurements were conducted along a northwest-southeast transect (long axis) through the center of the tarn on 2 August and daily from 4 to 8 August. Temperature and EC were measured every 2 m at three depths (center of the bottom third, middle third and top third of the water column). EC measurements were corrected to 25°C and converted to chloride concentration. Chloride concentration in the tarn (C_{tarn}) was assumed to equal the volume-weighted average of all chloride concentration measurements (both directly measured and calculated from EC) in three depth zones. Thus, C_{tarn} was determined as:

$$C_{tarn} = (C_1V_1 + C_2V_2 + C_3V_3)/(V_1 + V_2 + V_3) \quad (5)$$

where V_1, V_2, and V_3 are water volumes determined by dividing the tarn into three sections of equal depth. C_1, C_2, and C_3 are the arithmetic averages of chloride concentration for each corresponding volume.

[22] The uncertainty associated with C_{tarn} values was calculated as follows:

$$W_y = \sqrt{\left(\frac{V_1}{V_T} \times W_1\right)^2 + \left(\frac{V_2}{V_T} \times W_2\right)^2 + \left(\frac{V_3}{V_T} \times W_3\right)^2} \quad (6)$$

where W_y is the uncertainty in the volume-weighted average chloride concentration of the tarn (%), V_T is the total volume of the tarn, and W_1, W_2, and W_3 are the standard deviations of concentrations in each depth zone (expressed as a percentage of the arithmetic average) [*Genereux*, 1998]. This uncertainty ranged from 8.8 to 12%, with the exception of 6 August, for which the uncertainty was 16%.

[23] The change in chloride mass, $\Delta(C_{tarn}V)$, was then determined by:

$$\Delta(C_{tarn}V) = C_{tarn}(t_i)V(t_i) - C_{tarn}(t_{i-1})V(t_{i-1}) \quad (7)$$

where $C_{tarn}(t_i)$ is the tarn concentration at the ith time step as calculated by equation (5) and $V(t_i)$ is the volume of the tarn at the ith time step.

[24] The groundwater inflow was calculated by simultaneously solving equations (1) and (4):

$$GW_{in} = [\Delta(C_{tarn}V) - C_PP - C_{GWout}(\Delta V + E - P)]/(C_{GWin} - C_{GWout}) \quad (8)$$

from which GW_{out} was calculated using equation (1). Note that no precipitation was recorded during the experimental period (2–9 August) and consequently, P and C_PP were set to zero.

3.3. Energy Balance

[25] Groundwater flow into and out of the tarn results in the advection of energy. The energy balance of the East Tarn can be written as

$$Q_n + Q_a + Q_P + Q_E + Q_H + Q_{cond} = Q_w \quad (9)$$

where Q_n (J) is net radiation, Q_a (J) is net advection of energy by groundwater, Q_P (J) is the energy contribution due to precipitation, Q_E (J) is the latent heat, Q_H (J) is the sensible heat, Q_{cond} (J) is the energy exchange by conduction through the tarn bed, and Q_w (J) is the energy stored in the tarn. All terms are expressed as total energy over a time interval of computation. A positive sign of the terms in the left-hand side indicates addition of energy to the tarn. To collect the data required for energy balance calculation, an automatic weather station was installed in the tarn basin (see Figure 1c for location), equipped with sensors for air temperature and relative humidity (Vaisala, HMP45), radiation (Kipp & Zonen, CNR1), and wind speed and direction (RM Young, 05103). These values were measured every minute and recorded as 30 min averages using a datalogger (Campbell Scientific, CR1000).

[26] Due to difficult terrain and large fluctuations in tarn water levels, the radiometer could not be installed directly over the tarn surface to measure outgoing radiation directly. Therefore, net radiation was determined by measuring incoming shortwave (SW) and longwave (LW) radiation and calculating outgoing SW and LW radiation. Outgoing SW radiation was calculated using an albedo of 0.064 [*Cogley*, 1979]. Outgoing LW radiation (LW_{out}, W m^{-2}) was calculated using the Stefan-Boltzman equation:

$$LW_{out} = \sigma\varepsilon T_s^4 \quad (10)$$

where σ is the Stefan-Boltzman constant (5.67×10^{-8} W m^{-2} K^{-4}), ε is the emissivity of water (= 0.95) [*Oke*, 1988, p. 12], and T_s is the temperature of the tarn surface (K) as measured by a thermistor (Campbell Scientific 107B, accuracy ±0.2 K) shielded from direct solar radiation. Radiation components were measured or calculated in W m^{-2} and converted to J by multiplying the former by the area of tarn water surface (A) and the time interval of computation (Δt).

[27] The energy contribution to the tarn due to rainfall can be calculated as:

$$Q_P = Pc_w\rho_w(T_{rain} - T_{tarn}) \quad (11)$$

where ρ_w (kg m^{-3}) is the density of water, c_w (J kg^{-1} K^{-1}) is the specific heat of water, T_{tarn} is the average tarn temperature (°C), and T_{rain} is the temperature of rain (°C). However, equation (11) was not used in this study because no precipitation was recorded from 2 to 9 August.

[28] The latent heat flux was calculated as:

$$Q_E = -E\lambda_v\rho_wA\Delta t \quad (12)$$

where λ_v (J kg^{-1}) is the latent heat of vaporization. The Bowen ratio method was used to estimate the sensible heat flux from Q_E:

$$Q_H = \beta Q_E \tag{13}$$

where β is the Bowen ratio, calculated as:

$$\beta = \gamma(T_s - T_a)/(e_s - e_a) \tag{14}$$

where γ is the psychometric constant (kPa K^{-1}), T_a is air temperature measured ~2 m above the tarn water surface. In equation (14), e_s (kPa) is the vapor pressure of the tarn surface (assumed equal to the saturated vapor pressure) [*Dingman*, 2002, p. 274]:

$$e_s = 0.611 \exp[17.3T_s/(T_s + 273.3)] \tag{15}$$

and e_a is the vapor pressure of the air:

$$e_a = RH \times 0.611 \exp[17.3T_a/(T_a + 273.3)] \tag{16}$$

where RH is the relative humidity. The psychometric constant was calculated as:

$$\gamma = c_a P_a/(0.622\lambda_v) \tag{17}$$

where c_a is the specific heat of air (1.00×10^3 J kg^{-1} K^{-1}) [*Dingman*, 2002, p. 274] and P_a is the barometric pressure measured by a pressure sensor at the Lake O'Hara weather station located ~4 km from the tarn, and corrected for the elevation difference.

[29] The heat conduction term (Q_{cond}) was estimated by numerically solving the one-dimensional heat conduction equation [*Jury and Horton*, 2004, p. 176]. The top boundary condition at the water-sediment interface was given by the temperature recorded by a thermocouple (see below) at the sediment surface. The bottom boundary was set at a sufficient depth (10 m) below the tarn bottom to avoid the boundary effects. The annual mean soil temperature for 2008 at a 0.4 m depth in an ice-free region of the moraine ~200 m west of the tarn was 1.3°C (J. Hood, unpublished data, 2012). This was used as an estimate of the bottom boundary temperature, as well as the initial condition. The equation was first solved for 20 days of spin-up period using the average temperature of the tarn bottom during 24 July to 2 August as the constant top boundary condition, and then solved for the time period of 24 July to 9 August using the measured temperature for the top boundary. Thermal conductivity of saturated moraine material was calculated to be 1.5 Wm^{-1}K^{-1}, using the following equation from *Côté and Konrad* [2005]:

$$\lambda_{sat} = \lambda_s^{1-n}\lambda_w^n \tag{18}$$

where λ_{sat} is the saturated thermal conductivity of the material, λ_s is the thermal conductivity of the solid particles, assumed here to be limestone (3.4 Wm^{-1}K^{-1}), λ_w is the thermal conductivity of water (0.6 Wm^{-1}K^{-1}), and n is the porosity (estimated to be 0.3).

[30] The rate of change in energy storage in the tarn (Q_w in equation (9)) was calculated by:

$$Q_w = \Delta(T_{tarn}V)c_w\rho_w \tag{19}$$

where ρ_w is assumed constant.

[31] On 2 and 4–9 August, the tarn temperature was calculated from temperatures recorded during the transect surveys, using the same volume-averaging method described above (equation (5)). It was not possible to conduct the transect survey on 3 August, and thus, the tarn temperature was estimated from the vertical temperature profile measured by a string of copper-constantan thermocouples positioned every 0.2 m in the deepest region of the tarn. Uncertainty in the average tarn temperature values (determined using equation (6)) ranged from 6.7 to 12%, indicating that average tarn temperature (and therefore Q_w) was well constrained.

[32] The net advection component (Q_a) of the energy balance equations can be written as:

$$Q_a = c_w\rho_w[GW_{in}(T_{GWin} - T_0) - GW_{out}(T_{GWout} - T_0)] \tag{20}$$

where T_{GWin} is the temperature of the incoming groundwater and T_0 is the reference temperature (taken to be 0°C). We do not have direct measurements of the temperature of groundwater in the vicinity of the tarn, therefore the annual mean soil temperature of 1.3°C (see above) is assumed to represent T_{GWin}. This is within the temperature range (1.2–1.5°C) of groundwater measured during August and September of 2005 and 2006 at Groundwater Springs (see Figure 1b) by *Roy and Hayashi* [2009]. Estimation of T_{GWout} will be described in section 4.

[33] By simultaneously solving equations (1) and (9), groundwater flow into the tarn can be calculated as:

$$GW_{in} = [Q_a/(c_w\rho_w) - (\Delta V + E - P)T_{GWout}]/(T_{GWin} - T_{GWout}) \tag{21}$$

where Q_a is determined as:

$$Q_a = Q_w - Q_n - Q_P - Q_E - Q_H - Q_{cond}. \tag{22}$$

[34] Note that there was no precipitation during the experimental period and consequently, P and Q_P were set to zero.

3.4. Estimation of Hydraulic Conductivity

[35] The magnitude of groundwater inflow to and outflow from the tarn is related to the hydraulic conductivity of the moraine and the local hydraulic gradients. An objective of this study was to estimate the hydraulic conductivity at a scale of the entire tarn basin by quantitatively relating the groundwater flow rates with tarn water level. Several studies have used numerical groundwater flow models to refine our understanding of groundwater-surface water (GW-SW) interactions for shallow lakes by classifying lake-flow regimes and simulating the groundwater flow patterns near lakes [*Winter*, 1978; *Nield et al.*, 1994; *Townley and Trefry*, 2000; *Zlotnik et al.*, 2009]. Although these numerical models have the ability to resolve the complex geometry of pond and aquifer GW-SW exchange, they have

limited utility in this study due to the lack of detailed geological information and boundary conditions.

[36] Instead, this study uses a relatively simple analytical solution of *Kacimov* [2007], as summarized by *Zlotnik et al*. [2009], to represent a flow-through pond. The solution is for a simplified setting, in which a pond having an infinitely small depth is situated on top of a horizontal aquifer of infinite thickness (Figure 2a). In reality, lake-groundwater interaction occurs in unconfined aquifers. However, to obtain a closed-form solution, *Kacimov* [2007] linearized the flow equation by assuming the horizontal water table, meaning that the aquifer is treated as a confined system, similar to the common technique used by *Toth* [1962] and others. Two constant head boundaries placed far from the pond represent the regional hydraulic gradient (Figure 2b). The pond is represented by a constant head boundary, which alters the local piezometeric surface from the regional piezometric surface (Figurer 2b). Assuming a homogeneous, isotropic aquifer having hydraulic conductivity K (m s^{-1}), the groundwater inflow (Q_{in}) to and outflow (Q_{out}) from a circular pond is given by [*Zlotnik et al*., 2009, equation (19)]:

$$Q_{in} = Q_{out} = 2Kir^2 \tag{23}$$

where i is the magnitude of regional hydraulic gradient and r (m) is the pond radius.

[37] For this site, the tarn (i.e., pond) has an elongated shape (Figure 1c), which we represent here as an ellipse, and the aquifer has a finite thickness, which is expected to be comparable to or smaller than the pond radius (Figure 2). As a result, we modified the original solution and equation (23) becomes:

$$Q_{in} = Q_{out} = CKir_e^2 \tag{24}$$

where C is a dimensionless factor accounting for the effects of pond shape and aquifer thickness, and r_e is an effective radius defined as:

$$r_e = (A/\pi)^{1/2} \tag{25}$$

where A is the pond area as defined in equation (2).

[38] The ratio of the long axis to short axis of the tarn is roughly equal to 2 (Figure 1c), and the moraine aquifer thickness under the tarn is estimated to be roughly 10 m (see section 2). For these conditions, the value of C was estimated to be 2.0 using the numerical modeling approach of *Zlotnik et al*. [2009] (see Appendix B for details). Equation (24) is used with the measured flow rates and a plausible range of hydraulic gradient (see section 4) to estimate a range of K values for the coarse moraine material.

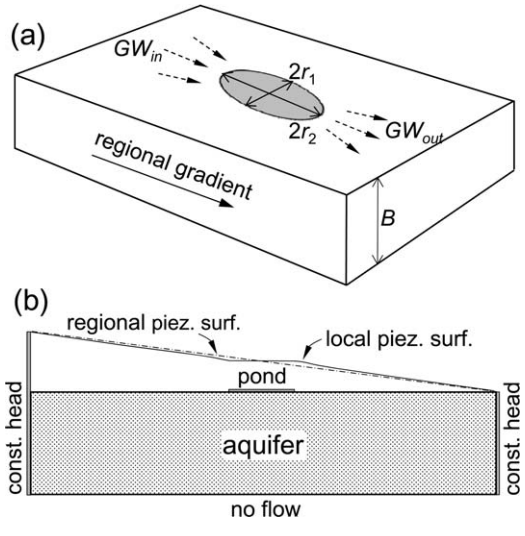

Figure 2. (a) Schematic diagram showing an ellipse-shaped pond (width $2r_1$, length $2r_2$) located on a horizontal aquifer having a thickness B. Dashed arrows indicate the direction of groundwater inflow (GW_{in}) and outflow (GW_{out}). (b) A longitudinal cross section through the middle of the pond showing the regional piezometric surface defined by constant head boundaries at the left and right, and the local piezometric surface. The pond is represented by a constant head boundary.

4. Results

4.1. Chloride Mass Balance

[39] The spatial distribution of chloride in the tarn is shown in the two-dimensional cross sections generated from the transect surveys (Figure 3) using the krigging interpolation method provided in the computer program Surfer 8 (Golden Software). The cross sections show some localization of chloride at the deepest regions of the tarn, suggesting that there may be a density effect causing high-concentration water to accumulate in these regions. However, there does not appear to be any consistent longitudinal trend in the spatial distribution of chloride, and in general, we interpret the chloride tracer within the tarn to be reasonably well mixed, particularly near the northwestern end of the tarn where groundwater outflow is expected to occur. Therefore, the average tarn concentration of chloride (C_{tarn}), calculated using equation (5), is used to represent the concentration of groundwater outflow (C_{GWout}) in the mass and water balance calculations below.

[40] Chloride concentration in the tarn decayed exponentially to pretracer release levels in ~5 days (Figure 4). Note that it was not possible to conduct a transect survey of chloride concentration on 3 August after the tracer release due to time constraints. Thus, the initial chloride concentration for the experiment (88 mg L^{-1}) was calculated from the amount of chloride added to the tarn and the volume of the tarn at the time of the tracer release.

[41] The calculated water balance for the tarn is presented in Table 1. Neither precipitation nor evaporation are included in Table 1, since no precipitation occurred during the experiment, and evaporation, which accounted for <1% of the daily water budget, was deemed a negligible component of the water balance. The calculated groundwater flow rates, in and out, were of a similar range; thus, their magnitude could not have been determined from the water balance alone, which only gives net groundwater flow. Groundwater flow out of the tarn calculated from the chloride mass balance ranged from 110 to 510 m^3 per time

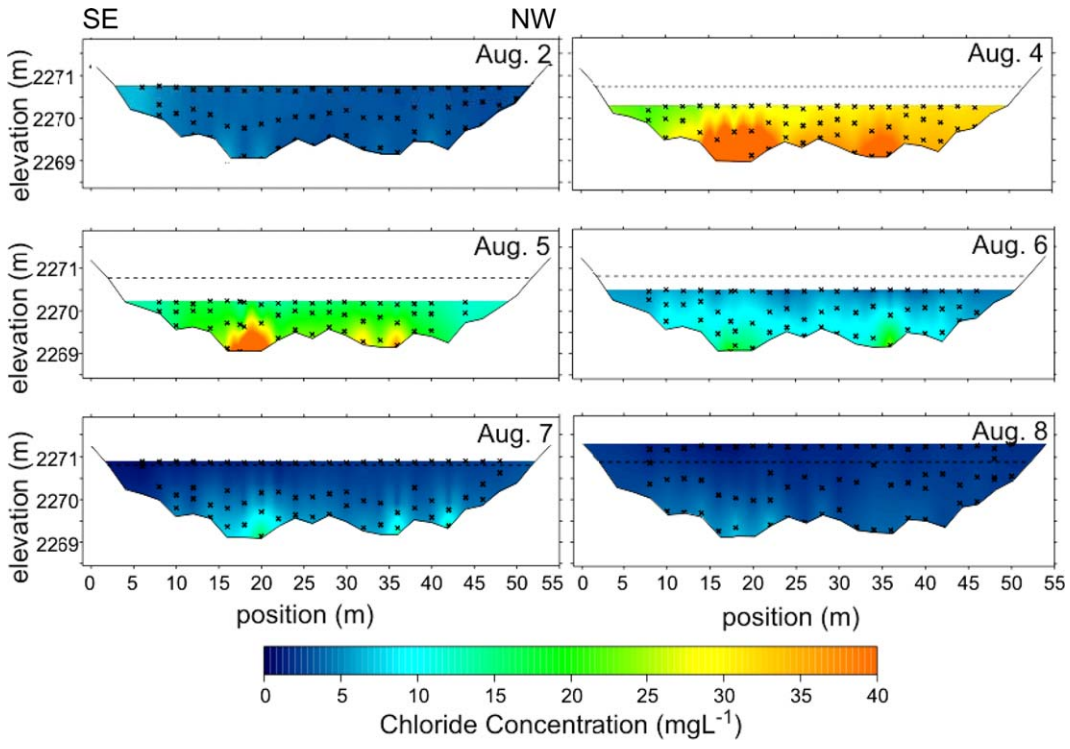

Figure 3. Two-dimensional profiles of chloride concentration within the tarn. The thick dashed line represents the water level at the start of the experiments (2 August), while the x's mark measurement locations. Groundwater flow direction is expected to be from left to right (SE to NW).

interval (~1 day), while daily average tarn water volume during this period ranged from 140 to 620 m^3. Therefore, daily groundwater flow through the tarn was on the same order of magnitude as the tarn volume.

4.2. Energy Balance

[42] The cross-section plot of water temperature for 2 August shows a lateral increase in temperature from ~3°C at the southeast end of the tarn to 5°C at the northwest end (Figure 5). This pattern suggests that the tarn acted as a flow-through system, with cool groundwater flowing into the south end of the tarn and gradually warming before flowing out of the tarn at the northwest end. This is consistent with the southeast-to-northwest direction of groundwater flow inferred from surface topography. As water level in the tarn decreased during 4–5 August, tarn temperature increased and became less variable. Thermal stratification developed (Figure 5) as the air temperature and water depth increased during 6–8 August (Figure 6). Due to the stratification, it would not be appropriate to use the average water temperature of the tarn (T_{tarn}) to represent the temperature of groundwater flowing out of the tarn (T_{GWout}) in equation (20). Therefore, the average temperature of the middle and bottom zones was used as T_{GWout} in the following water-energy balance calculation.

[43] During the 3–8 August study period, the energy balance for the tarn was largely controlled by the net radiation, energy storage, and advection terms (Table 2), although latent and sensible heat flux terms were also significant in the last two time intervals. Daily average evaporation rate varied between 0.4 mm to 2.9 mm d^{-1} with the highest value recorded on 7 August. The heat conduction term was only a minor component of the energy balance. Note that average tarn water temperature (approximated by the thermocouple string measurement) remained stable and even slightly decreased during the high air temperature (and

Table 1. The East Tarn Water Balance Calculated by Both the Chloride Mass Balance and the Energy Balance Methods[a]

Balance Period			Cl Mass Balance		Energy Balance	
Date	Time Interval	ΔV	GW_{in}	GW_{out}	GW_{in}	GW_{out}
4 August	8/3 15:30 to 8/4 16:00	−87	210	300	180	270
5 August	8/416:00 to 8/5 18:30	−37	72	110	180	210
6 August	8/5 18:30 to 8/6 16:50	85	200	110	250	170
7 August	8/6 16:50 to 8/7 17:50	190	430	240	380	190
8 August	8/7 17:50 to 8/8 16:30	210	720	510	560	350

[a]The variables are expressed as a volume (m^3). No precipitation occurred and evaporation was determined to be negligible (<1% of the daily water budget).

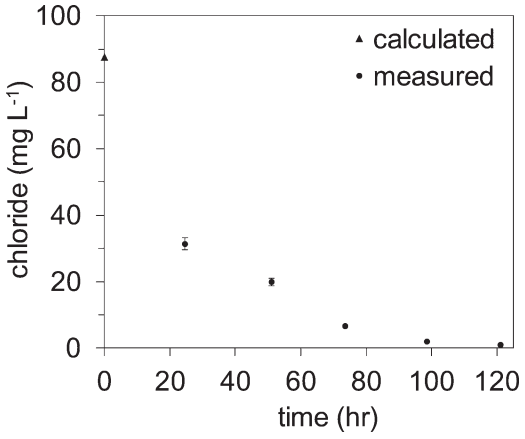

Figure 4. Average chloride concentration plotted against the time from the tracer release. Error bars represent the uncertainty in the calculated averages as determined from equation (5).

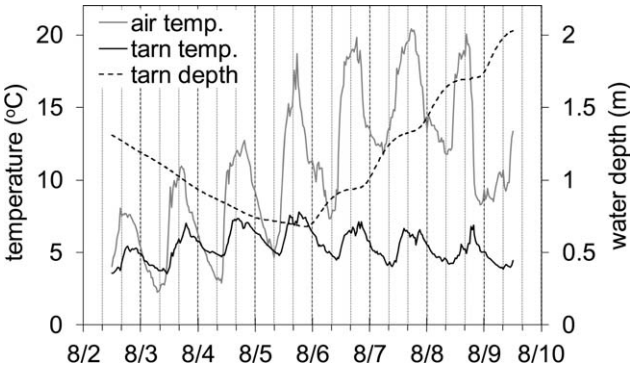

Figure 6. Comparison of tarn water temperature, air temperature, and tarn water depth. Gridlines are spaced at 8 h intervals with a major line indicating 0:00 of each day. Dates are shown in m/d format.

radiation) period of 6–8 August (Figure 6). This illustrates the strong effect that cold groundwater inflow has on energy balance.

[44] Groundwater flow rates into the tarn calculated from the water and energy balances ranged from 180 to 560 m^3 per time interval (~1 day), and groundwater outflow ranged from 170 to 350 m^3 (Table 1). These values are comparable to the values calculated from the chloride mass-balance approach (Table 1; also see Figure 7 for the comparison of flow rates expressed in $m^3\ d^{-1}$). Differences between the flow rates calculated by the two methods are likely caused by the uncertainty in measurements and estimations of mass and energy balance components (see section 5.1 for error analysis). Whether calculated using the chloride balance or energy balance method, the flow rates increased with tarn water level (see Figure 7c for the correlation between water level and GW_{out}). Increases in GW_{in} will add more water to the tarn, thus tending to raise the water level, which in turn will drive higher GW_{out}. In addition, it is expected that GW_{in} would be sensitive to the short-term variability of water input (e.g., snowmelt) in the up-gradient area, while GW_{out} would be largely driven by the hydraulic gradient between the tarn and the down-gradient aquifer connected to Opabin Lake.

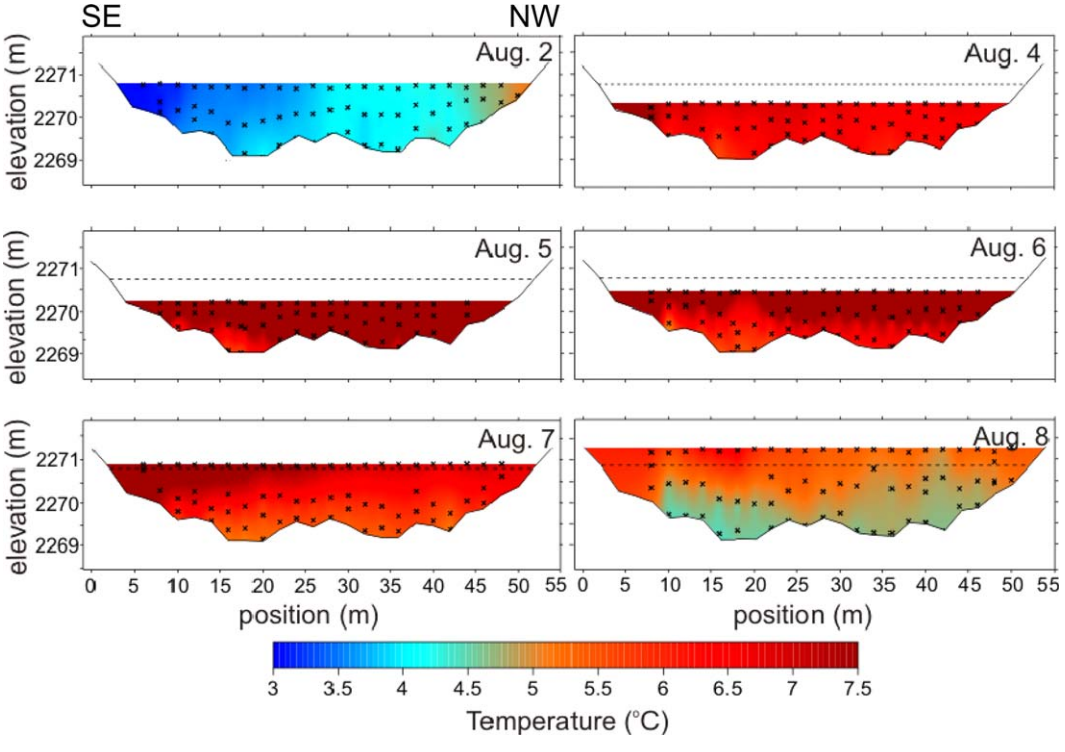

Figure 5. Two-dimensional profiles of tarn water temperature. The thick dashed line represents the water level at the start of the experiments (2 August), while the x's mark measurement locations.

Table 2. Daily Energy Balance of the East Tern[a]

Date	Q_a	Q_w	Q_n	Q_E	Q_H	Q_{cond}
4 August	−5.89	−1.60	5.09	−0.33	0.047	−0.52
5 August	−5.30	0.14	6.05	−0.40	0.21	−0.42
6 August	−3.53	1.78	5.97	−1.19	0.63	−0.11
7 August	−2.83	5.17	9.67	−3.18	1.55	−0.044
8 August	−4.69	1.94	7.85	−3.12	1.90	−0.008

[a]The unit for all variables is GJ, and the positive sign indicates an input of energy to water: advection (Q_a), storage (Q_w), net radiation (Q_n), latent heat (Q_E), sensible heat (Q_H), and conduction from the moraine (Q_{cond}).

4.3. Estimating Hydraulic Conductivity

[45] One objective of this study is to obtain an estimate of the hydraulic conductivity of the moraine at a scale of the entire tarn basin (10^3 m^2). To do this, we use equation (24), which relates groundwater flux out of the tarn to the size (r_e) and geometry (C) of the flow system, the hydraulic gradient (i), the hydraulic conductivity (K) of the moraine, and pond depth, given that the effective pond radius (r_e) is computed from pond depth using equations (2) and (25). Figure 8a shows the relationships between groundwater outflow and pond depth from both observed data (extracted from Figure 7c) and three predictions of equation (24) that bound the observed data. Note that the predictions take the form of increasing outflow with increasing water level, as was discussed above for the observations. This trial-and-error fitting of equation (24) to the observed data gives a range of values for CKi between 1.0 and 2.6 m d^{-1}, which translates to $Ki = 0.5$ to 1.3 m d^{-1} using $C = 2$ as a representative value (see section 3.4).

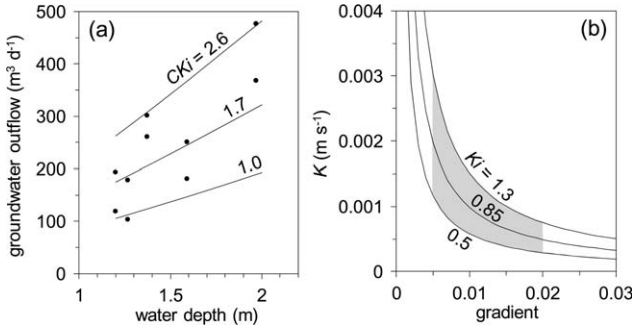

Figure 8. (a) Observed relation between the tarn water depth and groundwater outflow, and the relation predicted by equation (24) for three different values of CKi. (b) Relation between hydraulic conductivity (K) and gradient (i) for three different values of Ki corresponding to the three values of CKi in Figure 8a with $C = 2$. Shaded zone indicates a plausible range of gradient and K.

[46] An estimate of the regional hydraulic gradient (i) is needed to compute K from the above results, but it is difficult to estimate i because there is no groundwater observation well in the vicinity of the tarn. Using GPR, *McClymont et al*. [2012] detected the water table at an approximate elevation of 2270 m in Line 53 and 2268 m in Line 50 (see Figure 1b) on 15 July 2010. Dividing the difference in water-table elevation (2 m) by the distance between the two lines (220 m) gives an approximate gradient of 0.009 along the expected direction of groundwater flow. The East Tarn water level on the day of GPR survey was 2270.26 m, whereas the average East Tarn water level

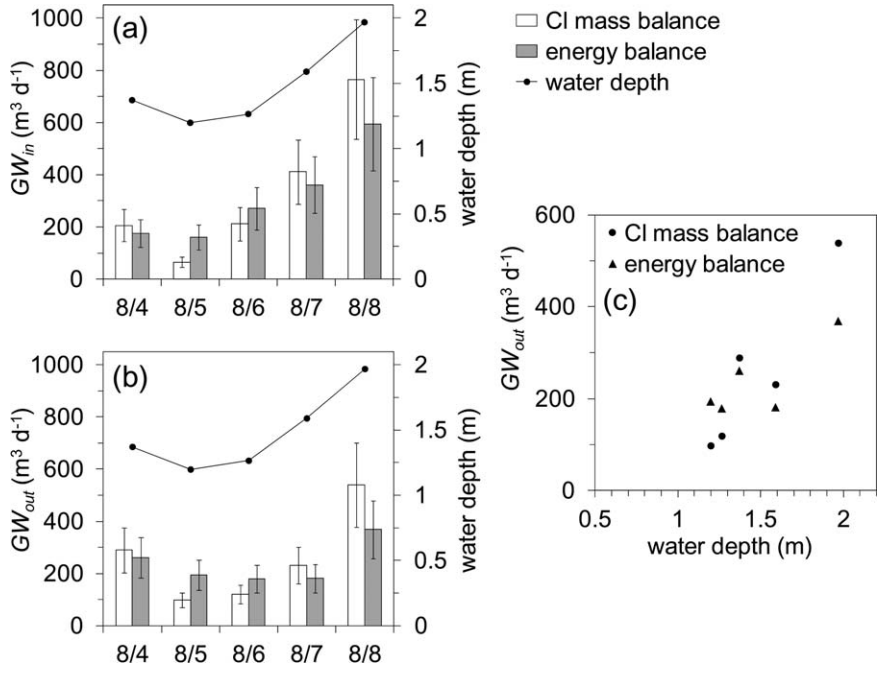

Figure 7. (a) A comparison of groundwater inflow (GW_{in}) as calculated by the chloride mass balance and the energy balance methods, and average tarn water depth. Error bars indicate 35% of flow rates, based on the error analysis in section 5.1. (b) Same comparison as in Figure 7a but for groundwater outflow (GW_{out}). (c) The relationship between GW_{out} and tarn water depth as calculated by the two methods.

during the 2008 tracer experiment was 2270.15 m. Therefore, the gradient estimated by the GPR data is expected to give a reasonable estimate of the regional gradient, even though the GPR survey was conducted two years after the present study. *McClymont et al*. [2012, Figure 6] also mapped the bedrock topography under the moraine complex and delineated a potential pathway of groundwater through a bedrock valley between the East Tarn region and Opabin Lake. An estimated length of this pathway is ~700 m. During the experimental period of 4–9 August 2008, the average difference in water level between the East Tarn and Opabin Lake was 6.5 m. Dividing this by 700 m gives a long-range gradient of 0.009, which is comparable to the gradient estimated from the GPR data. From these data, we expect the regional gradient around the tarn to be on the order of 0.005–0.02, considering the errors and uncertainties in water table elevation and flow path length.

[47] The relationship between K and i for the three calculated values of Ki that bound the observed data in Figure 8a are shown in Figure 8b. For the expected gradient range of 0.005–0.02, a plausible range of K is 0.3 to 3 $\times$ 10^{-3} m s^{-1}. This range is similar to values expected for coarse sands based on the Hazen formula that estimates K from grain size [e.g., *Fetter*, 2001, p. 86]. The K values determined in this study are higher than the range of values for "frontal moraine" (0.1 to 4 $\times$ 10^{-4} m s^{-1}) reported by *Parriaux and Nicoud* [1988], who did not describe the data source or measurement details, and the range of values (0.8 to 5 $\times$ 10^{-4} m s) for glacier forefield deposits in the Swiss Alps measured by *Magnusson et al*. [2013] using slug tests. The higher values may reflect the coarse nature of the proglacial moraine in the Lake O'Hara watershed, which is dominated by Cambrian quartzite rocks.

5. Discussion

5.1. Sensitivity and Error Analysis for Water Balances

[48] To assess the magnitude of uncertainty in mass and energy balance calculations, the sensitivity of estimated GW_{out} to changes in other variables is examined. For this purpose the sensitivity coefficient, f is defined as

$$f = (\Delta GW_{out}/GW_{out0})/(\Delta y/y_0) \quad (26)$$

where ΔGW_{out} is the amount of change in GW_{out} from the original value GW_{out0} and Δy is the amount of change in the other variable from the original value y_0. Thus, higher values indicate a greater sensitivity to uncertainty in a given parameter. The sensitivity coefficient was calculated for the mass balance and energy balance calculations for each day from 4 to 8 August (Table 3).

[49] The highest sensitivity coefficient values for the mass balance calculation were found for C_{tarn} and $\Delta(C_{tarn}V)$, indicating the importance of accurately measuring or estimating C_{tarn}. Note that the sensitivity values on 8 August are high because chloride concentration in the tarn had decreased to a very small value by this date (Figure 4). The estimated uncertainty in C_{tarn} is expected to be in the order of 20–30% based on the uncertainty associated with the calculation of C_{tarn} from the transect survey (equation (6)). The estimated uncertainty in ΔV is expected to be less than 10%. Since $\Delta(C_{tarn}V)$ is calculated from C_{tarn} and ΔV, we suggest that the error associated with this value is in the order of 20–30%. Given these ranges of uncertainty in estimated C_{tarn} and $\Delta(C_{tarn}V)$ and the magnitude of sensitivity coefficients for these variables (Table 3), the estimated error associated with mass balance calculations of GW_{out} is in the order of 30–40%.

[50] For the energy balance calculation, the highest sensitivity was found for Q_n (Table 3) but the radiation measurements have a relatively small magnitude of uncertainty (<10%). Therefore, the estimated uncertainty in GW_{out} associated with Q_n is in the order of 10–15%. The sensitivity coefficients for other parameters were relatively small, except for that for Q_w for 7 August. Sensible heat flux was calculated from evaporation flux and the Bowen ratio (equation (13)). While evaporation flux by the floating pan method is expected to have a relatively low magnitude of error (<20%), the Bowen ratio may have errors up to 50%. Assuming 50% as an uncertainty in Q_H, the uncertainty in the estimated GW_{out} associated with Q_H is in the order of 20–30%. Considering the uncertainty in all variables affecting the energy balance calculation, the uncertainty in the estimated GW_{out} is in the order of 30–40%.

[51] The sensitivity analysis above indicates the uncertainty in the estimated GW_{out} in the order of 30–40% for both chloride mass balance and energy balance methods. In comparison, the relative difference between the GW_{out} estimated by the two methods (Table 1) varies between 10% (4 August) and 49% (5 August) with the 5 day average of 29%, which is comparable to the uncertainty estimates derived from the sensitivity analysis (30–40%). The

Table 3. Sensitivity of Estimated Groundwater Outflow (GW_{out}) to Perturbation in the Groundwater Cl Concentration (C_{GWin}), Tarn Cl Concentration (C_{tarn}), Change in Tarn Water Volume (ΔV), and Change in Total Chloride Mass ($\Delta C_{tarn}V$) Used for the Chloride Mass Balance Method; and Net Radiation (Q_n), Energy Storage (Q_w), Temperature of Groundwater (T_{GWin}, T_{GWout}), Latent Heat (Q_E), and Sensible Heat (Q_H) Used for the Energy Balance Method[a]

	Cl Mass Balance				Energy Balance					
Date	C_{GWin}	C_{tarn}	ΔV	$\Delta(C_{tarn}V)$	Q_n	Q_w	T_{GWin}	T_{GWout}	Q_E	Q_H
4 August	0.03	−1.00	0	1.00	0.94	0.30	0.18	−1.29	−0.061	0.0088
5 August	0.035	−1.10	−0.02	1.00	1.19	−0.027	0.19	−1.25	−0.079	0.041
6 August	0.20	−1.10	0.10	0.90	1.50	−0.44	0.34	−1.25	−0.30	0.16
7 August	0.65	−1.40	0.25	0.70	2.52	−1.34	0.53	−1.29	−0.83	0.40
8 August	2.10	−2.65	0.60	0.40	1.34	−0.32	0.52	−1.35	−0.53	0.33

[a]Sensitivity coefficient is calculated for each balance period. A higher value indicates a greater sensitivity.

consistent results between the two independent methods give a confidence in the estimated values of groundwater flow rates and the hydraulic conductivity based on these values.

5.2. Characterizing the Groundwater Flow System

[52] Water balance calculations provide important information regarding groundwater-surface water interactions and the hydrologic response of the groundwater flow system. Depending on the hydrological setting, the flow regime of shallow groundwater-dominated lakes can be predominantly gaining ($GW_{in} >> GW_{out}$), predominantly losing ($GW_{in} << GW_{out}$), or a more balanced flow-through regime (i.e., a similar magnitude of GW_{in} and GW_{out}) [*Born et al.*, 1979; *Townley and Trefry*, 2000; *Zlotnik et al.*, 2009]. The East Tarn is a flow-through pond, as both GW_{in} and GW_{out} maintain similar values through the study period (Table 1). The temperature data profile for 2 August (Figure 5) suggests groundwater flows in from the southeast and leaves to the northwest, as mentioned previously.

[53] Flow-through ponds can have net groundwater inflow ($GW_{in} > GW_{out}$) or net groundwater outflow ($GW_{in} < GW_{out}$). The water balance results (Table 1) show that the East Tarn transitioned from a net groundwater outflow to net groundwater inflow condition during the period of study. This change was associated with increasing daytime and night temperatures and tarn water level (Figure 6), indications of increased snow or ice melt inputs (no rainfall was recorded) driving groundwater inflow. The influence of meltwater inputs with groundwater is apparent when a longer time frame is considered (Figure 9). In this case, given that the water balance of the East Tarn is dominated by groundwater flow (Table 1), the magnitude and sign of net groundwater flow are represented by the rate of change in tarn volume (dV/dt), as derived from the tarn water level (Figure 9c). During periods of increasing temperature (Figure 9a) and radiation (Figure 9b), such as the study period (4–9 August), the tarn water level showed a step-like pattern of increase, and dV/dt was positive (i.e., net inflow) with prominent diurnal fluctuations. A similar pattern occurred during 15–19 August. During colder periods with more muted radiation (e.g., 10–12 and 26–28 August), when melting would be reduced, the water level dropped and dV/dt became negative (i.e., net outflow) and more regular. These patterns further illustrate the strong response of the tarn to daily melt patterns, which is facilitated by changes in GW_{in}. Possible sources of melt water include the late-lying snow pack in Hungabee Cirque and the Opabin Glacier (Figures 1b and 1d).

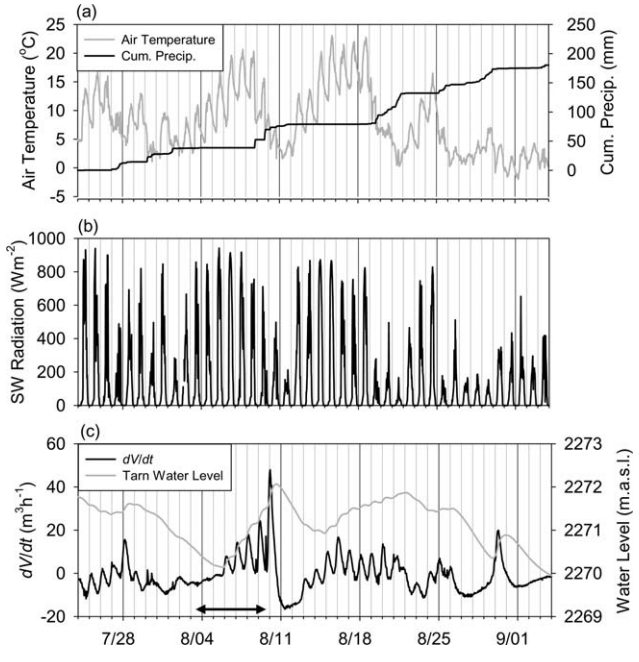

Figure 9. Comparison of (a) air temperature and cumulative precipitation, (b) incoming shortwave (SW) radiation, and (c) the water level and the rate of water-volume change (dV/dt) in the East Tarn. The thick horizontal line with arrows indicates the period of experiment. Grid lines indicate 0:00.

[54] Previous lake water balance studies in the Lake O'Hara watershed used equation (1) alone and hence were only able to estimate net groundwater flow [*Hood et al.*, 2006; *Roy and Hayashi*, 2008]. In this study, on a much smaller water body, both GW_{in} and GW_{out} were quantified with a reasonable confidence by simultaneously solving the water balance, solute mass balance, and energy balance equation. This more complete information is highly valuable for understanding the GW-SW interaction in proglacial environments. For example, the groundwater through-flow and the net groundwater flow can be compared with respect to the calculation of the nominal residence time of water (tarn volume divided by groundwater flow rate) in the East Tarn. The magnitude of groundwater through-flow can be represented in this case by taking the arithmetic average of GW_{in} and GW_{out}. Here each of GW_{in} and GW_{out} is estimated as the average of the values determined by the Cl mass balance and energy balance methods. Figure 10a shows the through-flow rates, the average of the two net groundwater flow rates determined by the two methods, and the average lake volume during each water balance period. The through-flow rates were substantially higher than the net groundwater flow, implying that using the net groundwater flow to represent GW_{in} [e.g., *Hood et al.*, 2006] could lead to an under-representation of GW-SW exchange. Figure 10b shows that using the through-flow rate results in a consistent residence time of ~1 day, whereas using the net groundwater flow gives a much longer and variable residence time.

6. Summary and Conclusions

[55] Two independent methods were used to estimate groundwater flow rates into and out of a tarn connected to a proglacial moraine aquifer. The first method is based on a full-tarn dilution experiment using a one-time injection of sodium chloride, and the second method involved detailed energy balance measurements to determine the advection of energy with groundwater flow between the tarn and aquifer. Although both methods showed considerable sensitivity to potential measurement errors, they produced similar results, providing confidence in the calculated values.

[56] Using a relatively simple semianalytical solution of the groundwater flow equation, representing a flow-through pond, with the calculated groundwater fluxes from this

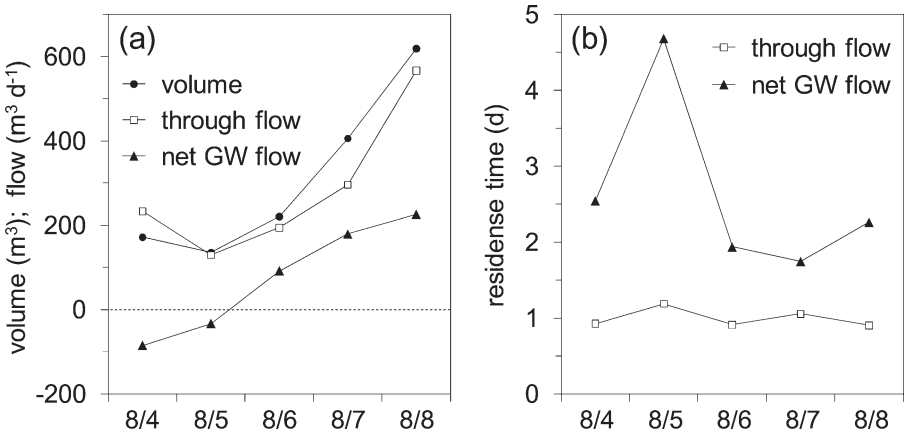

Figure 10. (a) Average tarn volume, groundwater through-flow, and net groundwater flow for each water balance period during 4–8 August. (b) Nominal residence time of water computed from the tarn volume divided by either throughflow or net groundwater flow.

study, hydraulic conductivity of unfrozen moraine material was estimated to be roughly in the order of 10^{-3} m s^{-1}. This calculation required estimating the hydraulic gradient from geophysical data and observations of other water bodies in contact with the moraine. This estimate represents the first attempt to date at quantifying the large-scale hydraulic conductivity of coarse moraine materials in an alpine environment. It should be applicable to proglacial moraines, and potentially other coarse deposits in alpine environments, derived from weathering-resistant quartzite and similar type of rocks.

[57] These methods provide a useful tool for examining groundwater-surface water interactions for small water bodies and for quantifying hydraulic properties of coarse-grained aquifers in rugged mountain environments where installation of monitoring wells is impossible or highly difficult. Such information is crucial for assessing the importance of groundwater flow in regulating the response of alpine headwater streams or lakes to meteorological forcing (i.e., glacier melt, snowmelt, and rain), particularly during base flow periods, for example. It can also provide insight into groundwater and surface water residence times, which affect biogeochemical processes and nutrient cycling in the aquatic system. For this site, the daily flow into and out of the tarn is on the same order of magnitude as the volume of the tarn itself, meaning that the nominal residence time of water in the tarn is ~1 day. Application of these methods, particularly in conjunction with geophysical techniques, to other alpine sites holds promise to generate more quantitative data that is needed to improve our conceptual and numerical models of these environments.

Appendix A

[58] The standard one-dimensional advection-dispersion equation [e.g., *Freeze and Cherry*, 1979, p. 389] is used to assess the relative magnitude of dispersive to advective transport of solutes through the pond bottom sediments. The equation can be written in a dimensionless form as:

$$\frac{\partial C_D}{\partial t_D} = \frac{\partial^2 C_D}{\partial x_D{}^2} - \frac{vL}{D}\frac{\partial C_D}{\partial x_D} \tag{A1}$$

where the dimensionless variables t_D, x_D, and C_D are defined as:

$$t_D = Dt/L^2 \quad x_D = x/L \quad C_D(x_D, t_D) = C(x,t)/C_0$$

where D (m^2 s^{-1}) is longitudinal dispersion coefficient, v (m s^{-1}) is linear flow velocity of groundwater, L (m) is the characteristic length of the system, C (x, t) (kg m^{-3}) is groundwater solute concentration, and C_0 (kg m^{-3}) is the solute concentration at the sediment surface (i.e., $x = 0$). The transport Peclet number (P_e) is defined by vL/D and indicates the relative importance of advection to dispersion. The longitudinal dispersion coefficient is given by:

$$D = D_m + \alpha_L |v| \tag{A2}$$

where D_m (m^2 s^{-1}) is the effective molecular diffusion coefficient and α_L (m) is longitudinal dispersivity, which is scale-dependent and can be estimated by [*Neuman*, 1990]:

$$\alpha_L = 0.0175 L^{1.46}. \tag{A3}$$

[59] Dividing the estimated groundwater inflow or outflow rates (Table 1) by the area of the pond gives a specific discharge on the order of 0.5–1 m d^{-1}. Assuming an effective porosity of 0.3, expected for coarse grain material, linear velocity is expected to be on the order of 1.7–3.3 m d^{-1}. Using this value of v with the length scale $L = 1$–2 m to represent the exchange of solutes between the pond water and the bottom sediments, equations (A2) and (A3) give P_e in a range of 40–60, indicating that advection is the dominant mode of transport.

[60] When the density of pond water is much higher than the underlying groundwater, buoyancy-induced free convection in the sediments may affect the pond-groundwater exchange. Whether or not free convection occurs depends on the Rayleigh number defined as [*Duffy and Al-Hassan*, 1988]:

$$R_a = KL(\Delta\rho/\rho)/(v\alpha_T) \tag{A4}$$

where $\Delta\rho$ (kg m^{-3}) is the density difference between pond water and groundwater, ρ (kg m^{-3}) is groundwater density,

and α_T (m) is vertical transverse dispersivity. *Duffy and Al-Hassan* [1988] used numerical experiments to show that the threshold value of R_a for free convection under closed basin lakes is on the order of 400–600. In the present study, the maximum concentration of chloride in the pond is ~40 mg L^{-1} (or 66 mg L^{-1} as NaCl), which gives a $\Delta\rho/\rho$ on the order of 6.5×10^{-5}. The K is estimated to be on the order of 10^{-3} m s^{-1}(Figure 8b), v is estimated to be 1.7–3.3 m d^{-1} (see above), and α_T is estimated to be roughly 10% of the α_L calculated from equation (A3). Using these values with $L = 1$–2 m in equation (A4) gives R_a on the order of 0.7–1.9, which is much lower than the threshold (400–600) reported by *Duffy and Al-Hassan* [1988]. Therefore, the effect of free convection is expected to be negligible in the present study.

Appendix B

[61] The coefficient C in equation (24) was numerically determined by steady-state flow simulations of a rectangular solid model domain (Figure 2a) using MODFLOW [*McDonald and Harbaugh*, 1996] within the software package Visual MODFLOW (Schlumberger Water Services), essentially following the approach of *Zlotnik et al*. [2009]. The length of model domain was 200 m and the width was 100 m. Preliminary simulations showed that this length and width were large enough to avoid the boundary effects for a pond with r_1 and r_2 ranging from 5 to 10 m. The thickness of the model domain (B) was varied to examine the effects of the ratio B/r_e on C. The vertical grid spacing varied from $\Delta z = 0.1$ to 0.5 m in the top 5 m, and 1–2 m in the rest. The horizontal grid spacing in the longitudinal direction was $\Delta x = 0.5$ m in the central region ($x = 90$–110 m), 1 m in the surrounding region ($x = 80$–90 and 110–120 m), and of 2 m in the rest. Similarly, the horizontal grid spacing in the transverse direction was $\Delta y = 0.5$ m in $y = 45$–55 m, 1 m in $y = 35$–45 and 55–65 m, and 2 m in the rest. Constant head boundaries were specified at $x = 0$ and 200 m to set up a regional hydraulic gradient of 0.01 across the model domain (Figure 2b). The pond is represented by a constant head boundary surface (Figure 2b), and the water flow in and out of the pond was calculated using the Zone Budget tool. The width of the elliptic pond was fixed at $2r_1 = 10$ m, while the length was varied between $2r_2 = 5$ m and 20 m to examine the effects of r_e and the pond orientation on C. The aquifer was assumed to be homogeneous and isotropic with $K = 0.001$ m s^{-1}.

[62] Figure A1 shows an example of simulated hydraulic head distribution and the extent of the zone influenced by pond-groundwater interaction (i.e., capture zone) for a case of $r_2 = 10$ m and $B = 14$ m ($r_e = 7.1$ m, $B/a_e = 2$, $r_2/r_1 = 2$). The width of the capture zone in the top model layer extends beyond the pond width (Figure A1a). The thickness of the capture zone in the longitudinal cross section at $y = 50$ m is much smaller than the depth of the aquifer (Figure A1b), indicating that the effects of bottom boundary is negligible in this case.

[63] As shown by *Zlotnik et al*. [2009], the relationship among flow, hydraulic conductivity, and gradient is independent of the absolute size of the model domain or values of hydraulic conductivity and gradient when results are expressed in dimensionless numbers. We define a dimensionless groundwater flow rate through the pond (Q_D) as:

$$Q_D = Q/Kir_e^2 \tag{A5}$$

where Q (m^3 s^{-1}) is the flow rate, i is the regional gradient, and a_e (m) is the characteristic length of the flow system defined by the effective radius of the pond [*Zlotnik et al*., 2009]. Comparison of equations (A5) and (24) indicates that $C = Q_D$.

[64] *Zlotnik et al*. [2009] showed that $Q_D = 2$ for a circular pond with a very large value of B/r_e (see equation (23)). Our simulations for a circular pond ($r_2/r_1 = 1$) gave $Q_D \cong 2$ for cases with large B/r_e (Figure A2), consistent with *Zlotnik et al*. [2009], and Q_D decreased for smaller values of B/r_e reflecting the influence of the bottom boundary.

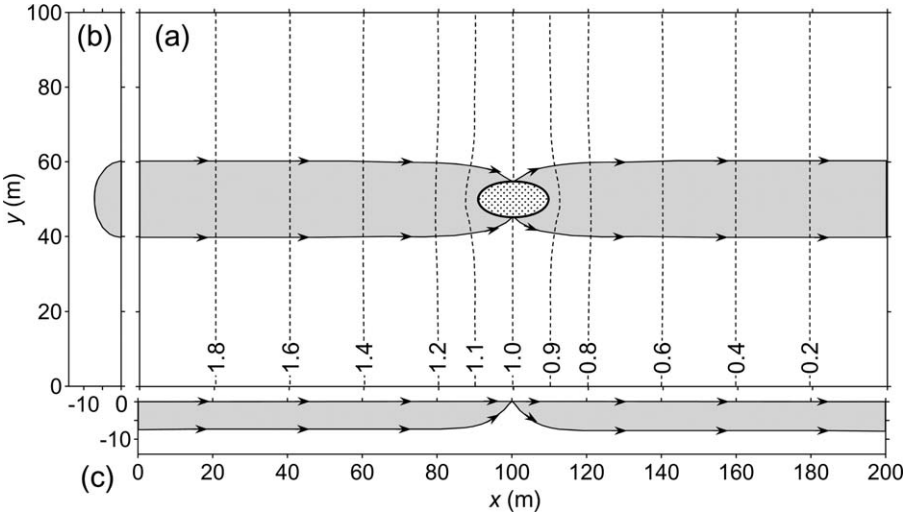

Figure A1. (a) Hydraulic head contours (1 m interval) and the extent of the flow capture zone in the top model layer, (b) transverse cross section at $x = 0$ showing the extent of the capture zone, and (c) longitudinal cross section at $y = 50$ m showing the extent of the capture zone.

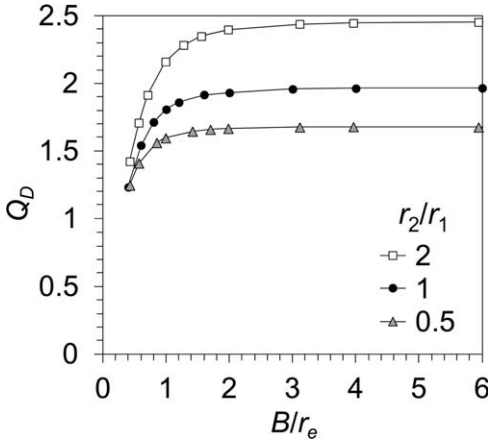

Figure A2. Relation between dimensionless flow rate (Q_D) and the ratio of aquifer thickness to effective pond radius (B/r_e) for various aspect ratios (r_2/r_1) of the ellipse.

Simulations for the elliptic pond with the long axis parallel to flow ($r_2/r_1 = 2$) gave Q_D that were greater compared to the circular-pond case, and the elliptic pond with the short axis parallel to flow ($r_2/r_1 = 0.5$) gave smaller Q_D (Figure A2).

[65] The East Tarn has an approximate aspect ratio (= long axis/short axis) of 2. The flow direction is somewhat uncertain, but the temperature distribution in the pond (Figure 5) shows that the flow has a strong component parallel to the long axis of the pond, suggesting that the condition is similar to the case with $r_2/r_1 = 2$. During the period of tracer experiment, the r_e calculated from the pond area (equation (25)) varied between 10 and 13.5 m, and the estimated aquifer thickness is 10 m, which gives B/a_e in a range of 0.74–1.0. Based on these data, an appropriate range of Q_D (and C) representing the pond in the present study is 1.9–2.1. We use the middle value of $C = 2.0$ for the estimation of K using equation (24).

[66] **Acknowledgments.** We gratefully acknowledge the help of dedicated field assistants who are too many to name. We also thank Jaime Hood for valuable discussion and for providing snowcover and soil temperature data, Parks Canada and Lake O'Hara Lodge for logistical support, and Chris Hopkinson for providing the digital elevation data. Funding was provided by Biogeoscience Institute (University of Calgary), Alberta Ingenuity Centre for Water Research, Canadian Foundation for Climate and Atmospheric Sciences (IP3 Network), Natural Sciences and Engineering Research Council of Canada, Environment Canada Science Horizons Program, and Alberta Ingenuity Scholarship to GL. Constructive comments and suggestions by the Associate Editor, Jeff McKenzie, and two anonymous reviewers improved the paper.

References

Andermann, C., L. Longuevergne, S. Bonnet, A. Crave, P. Davy, and R. Gloaguen (2012), Impact of transient groundwater storage on the discharge of Himalayan rivers, *Nat. Geosci.*, *5*, 127–132.

Anderson, M. P. (2005), Heat as a ground water tracer, *Ground Water*, *43*, 951–968.

Baraer, M., J. M. McKenzie, B. G. Mark, J. Bury, S. Knox, and S. Fortner (2009), Characterizing contributions of glacier melt and groundwater during the dry season in a poorly gauged catchment of the Cordillera Blanca (Peru), *Adv. Geosci.*, *22*, 41–49.

Barnett, T. P., J. C. Adam, and D. P. Lettenmaier (2005), Potential impacts of a warming climate on water availability in snow-dominated regions, *Nature*, *438*, 303–309.

Born, S. M., S. A. Smith, and D. A. Stephenson (1979), Hydrogeology of glacial-terrain lakes, with management and planning applications, *J. Hydrol.*, *43*, 7–43.

Brown, L. E., D. M. Hannah, A. M. Milner, C. Soulsby, A. J. Hodson, and M. J. Brewer (2006), Water source dynamics in a glacierized alpine river basin (Taillon-Gabiétous, French Pyrénées), *Water Resour. Res.*, *42*, W08404, doi:10.1029/2005WR004268.

Caballero, Y., V. Jomelli, P. Chevallier, and P. Ribstein (2002), Hydrological characteristics of slope deposits in high tropical mountains (Cordillera Real, Bolivia), *Catena*, *47*, 101–116.

Chikita, K., S. P. Joshi, J. Jha, and H. Hasegawa (2000), Hydrological and thermal regimes in a supra-glacial lake: Imja, Khumbu, Nepal Himalaya, *Hydrol. Sci. J.*, *45*, 507–521.

Clow, D. W., L. Schrott, R. Webb, D. H. Campbell, A. Torizzo, and M. Dornblaser (2003), Ground water occurrence and contributions to streamflow in an alpine catchment, *Colorado Front Range, Ground Water*, *41*, 937–950.

Cogley, J. G. (1979), Albedo of water as a function of latitude, *Mon. Weather Rev.*, *107*, 775–781.

Conant, B. (2004), Delineating and quantifying ground water discharge zones using streambed temperatures, *Ground Water*, *42*, 243–257.

Constantz, J. (2008), Heat as a tracer to determine streambed water exchanges, *Water Resour. Res.*, *44*, W00D10, doi:10.1029/2008WR006996.

Côté, J., and J.-M. Konrad (2005), Thermal conductivity of base-course materials, *Can. Geotech. J.*, *42*, 61–78.

Dingman, S. (2002), *Physical Hydrology*, Prentice Hall, Upper Saddle River, N. J.

Duffy, C. J., and S. Al-Hassan (1988), Groundwater circulation in a closed desert basin: Topographic scaling and climatic forcing, *Water Resour. Res.*, *24*, 1675–1688.

Elo, P. A.-R. (2007), The energy balance and vertical thermal structure of two small boreal lakes in summer, *Boreal Environ. Res.*, *12*, 585–600.

Fetter, C. W. (2001), *Applied Hydrogeology*, 4th ed., Prentice Hall, Upper Saddle River, N. J.

Freeze, R. A., and J. A. Cherry (1979), *Groundwater*, Prentice Hall, Englewood Cliff, N. J.

Genereux, D. (1998), Quantifying uncertainty in tracer-based hydrograph separations, *Water Resour. Res.*, *34*, 915–919.

Gurrieri, J. T., and G. Furniss (2004), Estimation of groundwater exchange in alpine lakes using non-steady mass-balance methods, *J. Hydrol.*, *297*, 187–208.

Hatch, C. E., A. T. Fisher, J. S. Revenaugh, J. Constantz, and C. Ruehl (2006), Quantifying surface water-groundwater interactions using time series analysis of streambed thermal records: Method development, *Water Resour. Res.*, *42*, W10410, doi:10.1029/2005WR004787.

Hayashi, M. (2004), Temperature-electrical conductivity relation of water for environmental monitoring and geophysical data inversion, *Environ. Monit. Assess.*, *96*, 119–128.

Hayashi, M., and G. van der Kamp (2000), Simple equations to represent the volume-area-depth relations of shallow wetlands in small topographic depressions, *J. Hydrol.*, *237*, 74–85.

Hopkinson, C., M. Hayashi, and D. Peddle (2009), Comparing alpine watershed attributes from LiDAR, photogrammetric, and contour-based digital elevation models, *Hydrol. Processes*, *23*, 451–463.

Hood, J. L., J. W. Roy, and M. Hayashi (2006), Importance of groundwater in the water balance of an alpine headwater lake, *Geophys. Res. Lett.*, *33*, L13405, doi:10.1029/2006GL026611.

Huss, M. (2011), Present and future contribution of glacier storage change to runoff from macroscale drainage basins in Europe, *Water Resour. Res.*, *47*, W07511, doi:10.1029/2010WR010299.

Jury, W., and R. Horton (2004), *Soil Physics*, 6th ed., John Wiley, Hoboken, New Jersey.

Kalbus, E., F. Reinstorf, and M. Schirmer (2006), Measuring methods for groundwater-surface water interactions: A review, *Hydrol. Earth Syst. Sci.*, *10*, 873–887.

Kacimov, A. R. (2007), Three-dimensional groundwater flow to a shallow pond: An explicit solution, *J. Hydrol.*, *337*, 200–206.

Krainer, K., and W. Mostler (2002), Hydrology of active rock glaciers: Examples from the Austrian Alps, *Arct. Antarct. Alp. Res.*, *34*, 142–149.

LaBaugh, J. W., T. C. Winter, D. O. Rosenberry, P. F. Schuster, M. M. Reddy, and G. R. Aiken (1997), Hydrological and chemical estimates of the water balance of a closed-basin lake in north central Minnesota, *Water Resour. Res.*, *33*, 2799–2812.

Langston, G., L. R. Bentley, M. Hayashi, A. McClymont, and A. Pidlisecky (2011), Internal structure and hydrological functions of an alpine proglacial moraine, *Hydrol. Processes*, *25*, 2967–2982.

Lickorish, W. H., and P. S. Simony (1995), Evidence for late rifting of the Cordilleran margin outlined by stratigraphic division of the Lower Cambrian Gog Group, Rocky Mountain Main Ranges, British Columbia and Alberta, *Can. J. Earth Sci.*, *32*, 860–874.

Liu, F., M. W. Williams, and N. Caine (2004), Source waters and flow paths in an alpine catchment, Colorado Front Range, United States, *Water Resour. Res.*, *40*, W09401, doi:10.1029/2004WR003076.

Lowry, C. S., S. P. Loheide, C. E. Moore, and J. D. Lundquist (2011), Groundwater controls on vegetation composition and patterning in mountain meadows, *Water Resour. Res.*, *47*, W00J11,doi:10.1029/2010WR010086.

Magnusson, J., F. Kobierska, S. Huxol, M. Hayashi, T. Jonas, and J. W. Kirchner (2013), Melt water driven stream and groundwater stage fluctuations on a glacier forefield (Dammagletscher, Switzerland), *Hydrol. Processes*, doi:10.1002/hyp.9633, in press.

McClymont, A. F., M. Hayashi, L. R. Bentley, and J. Liard (2012), Locating and characterising groundwater storage areas within an alpine watershed using time-lapse gravity, GPR and seismic refraction methods, *Hydrol. Processes*, *26*, 1792–1804.

McDonald, M., and A. Harbaugh (1996), A modular three-dimensional finite difference groundwater flow model, *U.S. Geol. Surv. Open File Rep.*, *96-485*.

Neuman, S. P. (1990), Universal scaling of hydraulic conductivities and dispersivities in geologic media, *Water Resour. Res.*, *26*, 1749–1758.

Nield, S. P., L. R. Townley, and A. D. Barr (1994), A framework for quantitative analysis of surface water-groundwater interaction: Flow geometry in a vertical section, *Water Resour. Res.*, *30*(8), 2461–2475.

Oke, T. (1988), *Boundary Layer Climates*, 2nd ed., Routledge, New York.

Parriaux, A. and G. F. Nicoud (1988), Hydrological behaviour of glacial deposits in mountainous areas, *IAHS Publ.*, *190*, 291–312.

Parsons, D. F., M. Hayashi, and G. van der Kamp (2004), Infiltration and solute transport under a seasonal wetland: Bromide tracer experiments in Saskatoon, *Canada, Hydrol. Processes*, *18*, 2011–2027.

Price, R., D. Cook, J. Aitken, and E. Mounjoy (1980), Geology, Lake Louise, Alberta and British Columbia, *Geol. Surv. of Canada*, Ottawa.

Rodríguez-Rodríguez, M., E. Moreno-Ostos, I. De Vicente, L. Cruz-Pizarro, and S. L. R. Da Silva (2004), Thermal structure and energy budget in a small high mountain lake: La Caldera, *Sierra Nevada, Spain, N. Z. J. Mar. Freshwater Res.*, *38*, 879–894.

Rouse, W. R., P. D. Blanken, N. Bussières, C. J. Oswald, W. M. Schertzer, C. Spence, and A. E. Walker (2008), An investigation of the thermal and energy balance regimes of Great Slave and Great Bear Lakes, *J. Hydrometeorol.*, *9*, 1318–1333.

Roy, J. W., and M. Hayashi (2008), Groundwater exchange with two small alpine lakes in the Canadian Rockies, *Hydrol. Processes*, *22*, 2838–2846.

Roy, J. W., and M. Hayashi (2009), Multiple, distinct groundwater flow systems of a single moraine-talus feature in an alpine watershed, *J. Hydrol.*, *373*, 139–150.

Schmidt, C., B. Conant Jr., M. Bayer-Raich, and M. Schirmer (2007), Evaluation and field-scale application of an analytical method to quantify groundwater discharge using mapped streambed temperatures, *J. Hydrol.*, *347*, 292–307.

Siegel, D. (2008), Reductionist hydrogeology: Ten fundamental principles, *Hydrol. Processes*, *22*, 4967–4970.

Tague, C., and G. E. Grant (2009), Groundwater dynamics mediate low-flow response to global warming in snow-dominated alpine regions, *Water Resour. Res.*, *45*, W07421, doi:10.1029/2008WR007179.

Tenthorey, G. (1992), Perennial névés and the hydrology of rock glaciers, Permafrost Periglac. *Processes*, *3*, 247–252.

Toth, J. (1962), A theory of groundwater motion in small drainage basins in central Alberta, Canada, *J. Geophys. Res.*, *67*, 4375–4387.

Townley, L. R., and M. G. Trefry (2000), Surface water-groundwater interaction near shallow circular lakes: Flow geometry in three dimensions, *Water Resour. Res.*, *36*, 935–948.

Viviroli, D., H. H. Dürr, B. Messerli, M. Meybeck, and R. Weingartner (2007), Mountains of the world, water towers for humanity: Typology, mapping, and global significance, *Water Resour. Res.*, *43*, W07447, doi:10.1029/2006WR005653.

Williams, M. W., M. Knauf, N. Caine, F. Liu, and P. L. Verplanck (2006), Geochemistry and source waters of rock glacier outflow, Colorado Front Range, Permafrost Periglac. *Processes*, *17*, 13–33.

Winter, T. C. (1978), Numerical simulation of steady state three-dimensional groundwater flow near lakes, *Water Resour. Res.*, *14*, 245–254.

Zlotnik, V. A., F. Olaguera, and J. B. Ong (2009), An approach to assessment of flow regimes of groundwater-dominated lakes in arid environments, *J. Hydrol.*, *371*, 22–30.